Computational Engineering and Physical Modeling 4-4 (2021) 94-108

Contents lists available at **CEPM**

Computational Engineering and Physical Modeling

Journal homepage: www.jcepm.com

Vehicle Bridge Interaction Analysis on Concrete and Steel Curved Bridges

Y. Ye[1], C.C. Fu[2], X. Huang[3]

1. Research Assistant, the Bridge Engineering Software and Technology (BEST) Center, Department of Civil and Environmental Engineering, University of Maryland, College Park, MD 20740 USA
2. Research Professor and Director, the Bridge Engineering Software and Technology (BEST) Center, Department of Civil and Environmental Engineering, University of Maryland, College Park, MD 20740 USA
3. Associate Professor, College of Civil Engineering, Fuzhou University, Fuzhou 350116, China

Corresponding author: engineerferret@gmail.com

https://doi.org/ 10.22115/CEPM.2021.272934.1155

ARTICLE INFO

Article history:
Received: 21 February 2021
Revised: 23 November 2021
Accepted: 23 November 2021

Keywords:
Curved bridge;
Vehicle-bridge interaction;
Impact factor;
Curvature of radius;
Bridge surface roughness;
Traffic eccentricity and speed;
Empirical equation.

ABSTRACT

This study investigation is intended to research the dynamic response of horizontally curved bridges under heavy vehicle loads. Most of the main factors that affect the bridge dynamic response due to moving vehicles are considered. An improved 3D grid model, based on commercial software ANSYS Mechanical APDL, is developed for the analysis of curved bridges following the 3D shear-flexibility grillage analyzing method. A simplified numeric method, considering the effect of random road roughness and its velocity term, is developed for solving the interaction problem. With the model and numerical method presented, a series of parametric studies are conducted to study the curved bridge dynamic interaction. Based on the investigation of determining factors of curve bridge dynamic interaction, the expression of the upper-bound envelop for impact factors of maximum deflection is given with different surface conditions and highway speed limits as a function of bridge fundamental frequency or bridge central angle. A study is conducted on comparing these empirical equations and serval other major design codes, comments and suggestions are then made based on the discoveries.

How to cite this article: Ye, Y., Fu, C. C., & Huang, X. (2021). Vehicle Bridge Interaction Analysis on Concrete and Steel Curved Bridges. Computational Engineering and Physical Modeling, 4(4), 94–108. https://doi.org/10.22115/cepm.2021.272934.1155

1. Introduction

Although considerable deal of research has been done on the coupling vibration of bridge, most of the previous researches focused on straight girder bridges. Fewer studies have been done on the impact effect of curved bridges [1]. Engineers do not have full understanding of the influencing factors of vehicle bridge coupled vibration of curved bridges, and further research is needed. Besides, the current impact factor for traffic load on highway does not reflect the influence from the grade of bridge surface roughness. However, surface roughness is proven by majority of researchers to have a great impact on the vehicle dynamic load [2]. Whether the bridge dynamic response can be covered by a unified impact factor calculation formula, and whether the existing impact factor formula can be directly applied to the curved bridge, such problems have no answers yet. More theoretical studies are needed in order to provide a practical empirical formula to improve the design theory of curved bridges and maintenance and retrofit methods for existing curved bridges [3].

The specific objective of this research is to study the curved bridge dynamic response under vehicle-bridge interaction. First, by using commercial program ANSYS, several multi-beam models of existing bridges were built based on the shear force flexible grillage method. Both the warping stiffness and moment of inertia are considered in this model. A spatial vehicle model with 24 degrees of freedoms (DOFs) with three-dimensional (3D) beam element, mass element and spring-damper elements is adopted in the model. Taking effect of random surface roughness, the separation iteration algorithm is used to the coupled vibration of the two subsystems [4]. Second, using the model proposed above, this research analyzes the influence of vehicle speed, surface roughness, radius of curvature, lane eccentricity, stiffness and damping of tires and bridge structure, in order to fully understand the influence factors of dynamic response of curved bridges. Also, the influence of multi-lane loading, vehicle number and vehicle spacing on the impact factor are studied.

2. Vehicle-bridge interaction model

2.1. Simplified vehicle model

In this study, a typical 3-axle vehicle is simplified into a vibration system connected by mass, spring and damper. The vehicle body is modeled as a rigid body, and the suspension system and tire are modeled jointly by a spring and a viscous damper with energy dissipation capability. The mass of the suspension system and tire is simulated by the ideal mass elements. The model considers the vertical and horizontal vibrations of the vehicle and the rotational vibration around the three axes. The simplified model of the vehicle is shown in the figure below (Figure 1). The model is based on two connected “half-truck” model, each contains a total of 12 generalized degrees of freedom. Among them, four generalized coordinates of $y_m, z_m, \theta_{xm}, \theta_{ym}$ are selected to describe the lateral vibration, vertical vibration, roll around the x axis and pitch vibration around the y axis. The vertical and lateral vibration from front axle is described as z_1, y_1. The vertical vibration, lateral vibration, rolling and pitching behaviors of the rear suspension are described as $z_2, z'_2, z_3, z'_3, y_1, y_2$.

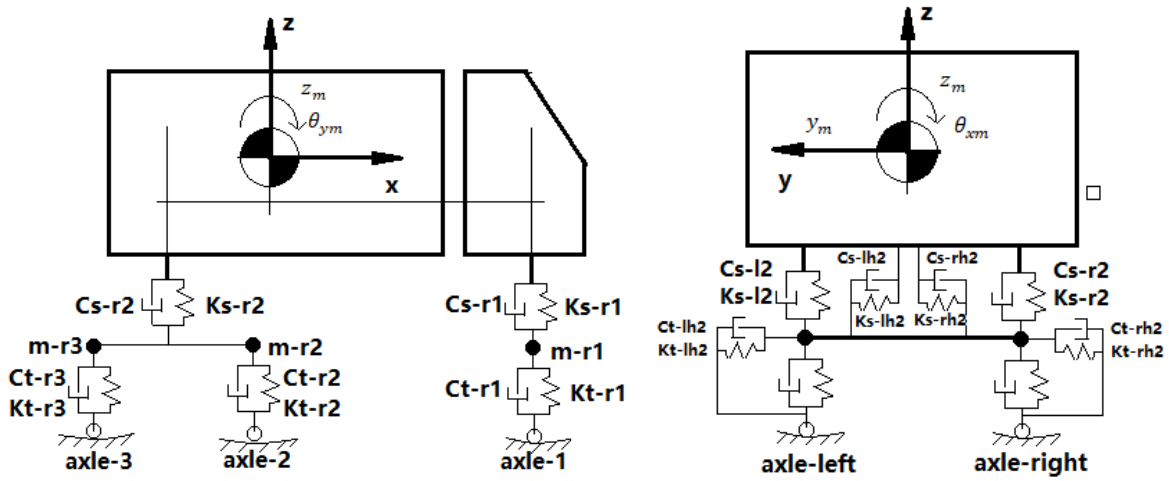

Fig. 1. 3D truck model side view (left) and rear view (right).

2.2. Random surface roughness

It is assumed that the roughness of the pavement is a Gaussian random process with power spectrum to represent the statistical characteristics of the pavement. In this study, analysis chooses method developed by Eui-Seung Hwang and Wewak [5,6],

$$S_r(\Omega) = \begin{cases} \alpha\Omega_k^{-\beta} & \Omega_L < \Omega_K < \Omega_U \\ 0 & otherwise \end{cases} \tag{1}$$

Where

Ω – Spatial frequency, the inverse of the wavelength, indicating the number of occurrences of a harmonic in each meter, within the lower (L) and upper (U) bounds.

After applying inverse fast Fourier transform (FFT) to above formula, the vertical distribution function of the vertical irregular shape of the bridge deck can be obtained.

$$r(s) = \sum_{K=1}^{N} \alpha_K \, COS(2\pi\Omega_k \, s + \phi_k) \tag{2}$$

2.3. vehicle bridge coupling analysis

In the current study, the models used for vehicle bridge interaction analysis follow these assumptions.

1. When a vehicle travels along a curved bridge, the instantaneous center of rotation coincides with the center of curvature of the circular curve, and the deflection angle of the inner steering wheel is greater than the deflection angle of the outer steering wheel.

2. The vehicle lateral slip angle of the center of mass does not change with time and the vehicle makes a steady circular motion on the circumference. Also, the attack angle of the vehicle front wheel remains constant.

3. This study ignores the elastic deformation of the vehicle body, the suspension and axle. The vehicle body, suspension and axle are treated as rigid bodies where they are connected by springs and dampers. Dampers are assumed to have linear viscous damping property.

4. The body, the suspension and each pair of rigid bodies of the wheelset make small displacement vibration at the balance position and do not consider the influence of the change of the vehicle center of gravity height on the centrifugal force and the centrifugal moment caused by the slight vibration generated by the vehicle body under the unevenness of the bridge deck (Figure 2).

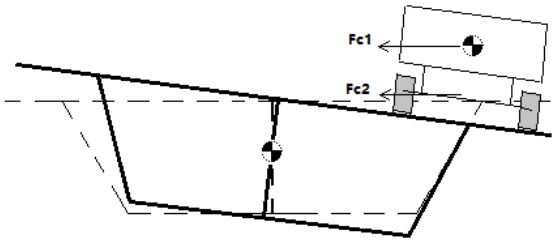

Fig. 2. Centrifugal forces on the moving vehicle.

5. The vehicle model is symmetrical along the longitudinal direction; the model ignores the vibration along the longitudinal axis. The rear wheels are travelling on the ruts of the front wheels.

2.4. Motion equations

Based on the commercial finite element analysis software ANSYS, the spring-damping element, mass element and the rigid rod space rod element are used to simulate the components of the vehicle. The vehicle model is discretely modeled according to the finite element method. The vibration equation of the vehicle can be expressed as [7–10].

$$m_v z'' + c_v z' + k_v z = f_v \tag{3}$$

The bridge model is discretized by the finite element method, the equation of motion of bridge is,

$$[M_b]\{\delta''\} + [C_b]\{\delta'\} + [K_b]\{\delta\} = [P_b] \tag{4}$$

To simplify the global damping matrix, the $[C_b]$ is usually taken as

$$[C_b] = \alpha[M_b] + \beta[K_b] \tag{5}$$

The factors α and β can be obtained by,

$$\alpha = (2\omega_1\ \omega_2\ (\xi_1\omega_2 - \xi_2\omega_1))/(\omega_2^2 - \omega_1^2)$$

$$\beta = \frac{2(\xi_2\omega_2 - \xi_1\omega_1)}{\omega_2^2 - \omega_1^2} \tag{6}$$

2.5. Centrifugal force effect

When a vehicle travelling in a uniform circular motion, centrifugal force $m_v v^2/\rho$ and moment $m_v v^2 h/\rho$ will apply to the mass center of the vehicle. During the circular motion, the mass center will have a lateral displacement $h\,sinx$ (hx). The total moment can be expressed as [5,7,11,12].

$$M = \frac{m_v v^2 h}{\rho} + m_v g h x \tag{7}$$

Assume the distances between vehicle mass center to the front and rear suspension centers to be l_V, l_H. The centrifugal forces for front and rear suspensions would be $m_v v^2 l_v/(\rho l)$ and $m_v v^2 l_H/(\rho l)$.

2.6. Bridge deck roughness effect

Assuming that the wheels and the deck are always in contact with each other when the vehicle runs through the bridge, the wheel and bridge contact points can be used to generate the dynamic load of the bridge. The dynamic loading between wheels and bridge can be written as [1,13–17].

$$F_{dij} = c_{tij}\left[z'_{sij} - \zeta'_{tij}(s,t) - r'(s_{ij})\right] + k_{tij}\left[z_{sij} - \zeta_{tij}(s,t) - r(s_{ij})\right] \tag{8}$$

$r(s_{ij})$ represents the roughness at given location

The external excitation due to surface roughness can then be expressed as.

$$f_{vij} = c_{tij}\left[\frac{\partial \zeta_{tij}(s,t)}{\partial t} + v\frac{\partial r(s)}{\partial s}\right] + k_{tij}\left[\zeta_{tij}(s,t) + r(s)\right] \tag{9}$$

3. Numerical study

To study the vehicle-bridge dynamic analysis, Manchuria concrete bridge in China was selected in the preliminary study to be modeled in ANSYS.

Manchuria Interchange is a cross-over bridge with a deck width of 12m, carriageway of 11m and a 6% cross-slope. The superstructure adopts a prestressed concrete continuous curved box girder with a curve radius of 280m. The main girder is a single-box double-chamber section with a beam height of 1.90m. The whole structure is a consolidation of pier and beam rigid frame system. The lower structure is a ribbed platform, the foundation of the pier is a rock-fill pile foundation, and the abutment adopts a basin rubber bearing as shown in Figure 3a.

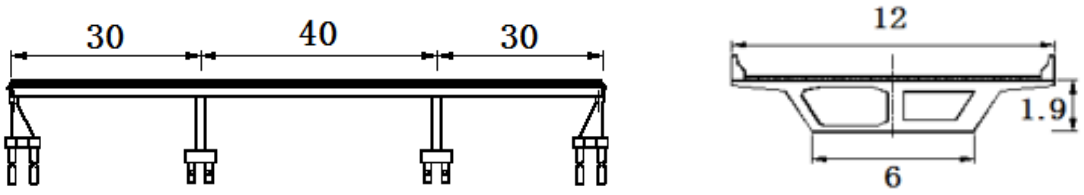

(a). Layout and cross section.

(b). Triple-beam model.

Fig. 3. Manchuria Bridge.

The three-beam dynamic analysis model (Figure 3b) reasonably distributes the mass and stiffness of the deck system to the middle and two side beams according to a certain equivalent method. Based on this, the mass distribution and cross-section characteristics of each main beam in the model are determined. The stiffness of the horizontal beam is related to the spacing b_1 of the girder. The horizontal beam is modeled by a massless element. Piers are fixed at the bottom where both ends of the main beam only constrained the vertical displacement.

To study the influence of bridge surface roughness during vehicle-bridge interaction. Three sets of bridge deck roughness profiles are generated in randeom and applied during the dynamic analysis: [16]: 1) Good surface condition ($a = 0.18 \times 10^{-6} m^3/circle$), 2) normal surface condition ($a = 2.5 \times 10^{-6} m^3/circle$), and 3) poor surface condition ($a = 10 \times 10^{-6} m^3/circle$). Additional profile of perfect surface condition (smooth surface) is also modeled for comparison purpose.

4. Preliminary study results

A preliminary study is conducted to understand the potential contributor of vehicle-bridge interaction problem. Figure 4 summarizes the influence of vehicle traveling speed to the dynamic amplication factors. It can be noticed that as the speed increased, the impact also increased slightly.

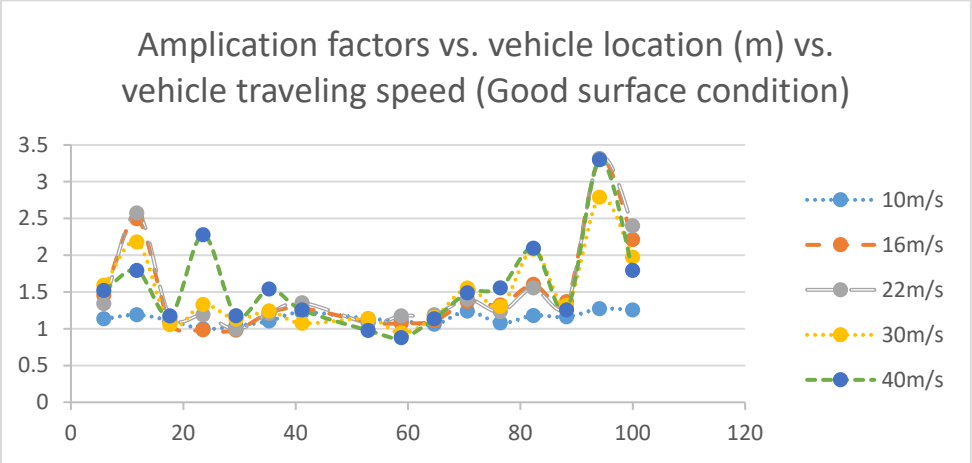

Fig. 4. Amplication factors of different traveling speeds.

Figure 5 shows bridge dynamic response when a 3-axle truck travels at outside with different surface conditions at the speed of 20m/s. By comparing displacement charts from different surface condition, the influence of surface condition to bridge dynamic response can be observed.

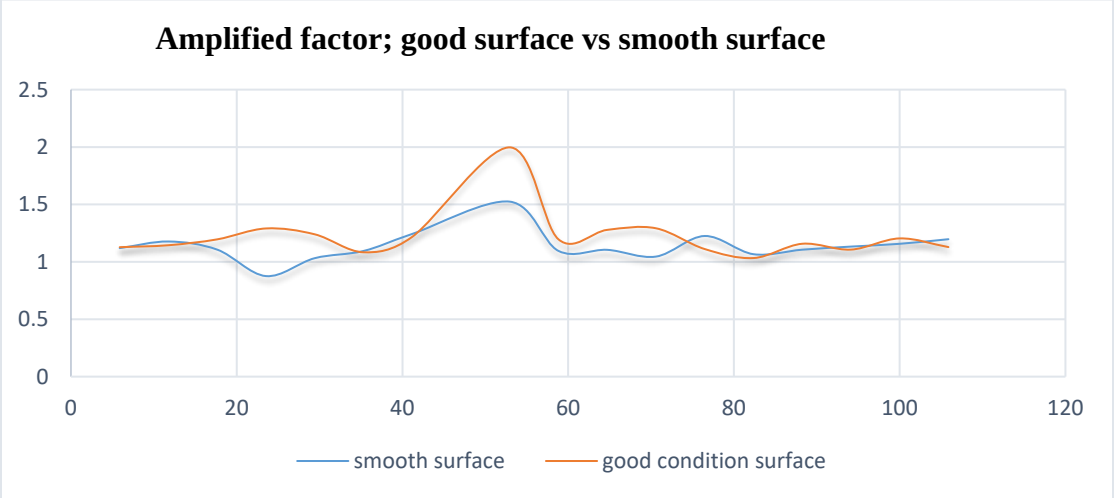

Fig. 5. Amplified factor at different surface conditions.

Additional hypothetical straight bridge with the same bridge properties is modeled to observe and compare the influence of curved bridge layout in the bridge vehicle interaction. The detailed comparion is shown in Figure 6. The impact factor comparison shows that the curved bridge has a noticable increament comparing to the straight one. It is reasonable to draw the conclusion that the curved bridge layout has increased the vehicle bridge interaction.

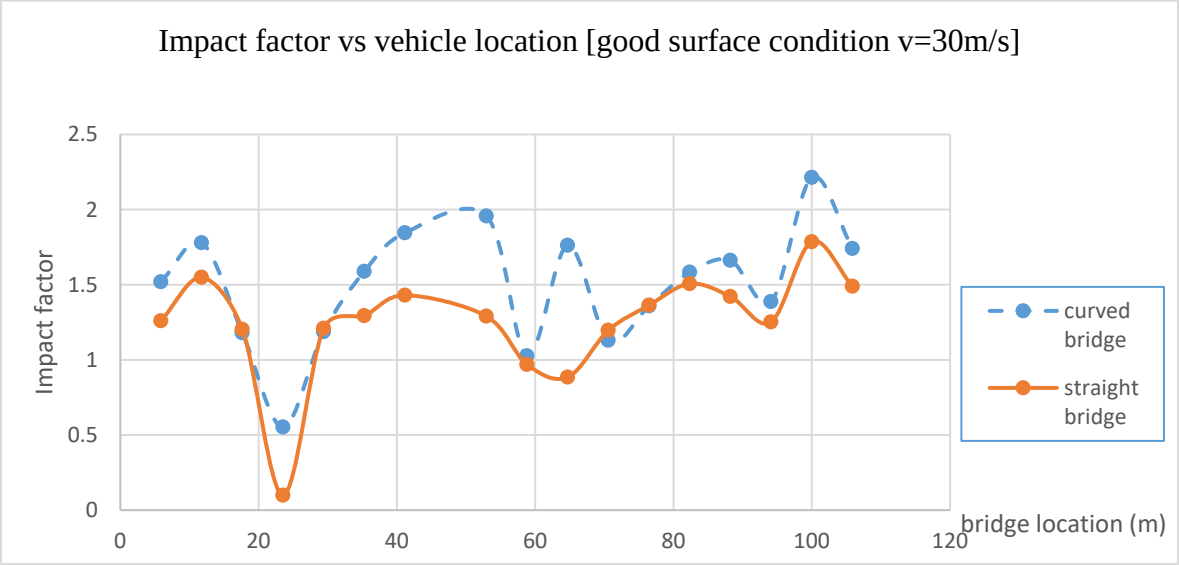

Fig. 6. Impact factor comparison between curved and hypothetical straight Manchuria Bridge.

By examining the bridge responses, it can be observed that the dynamic interaction of a curved bridge could be greatly influenced by various factors. As the vehicle travelling speeds increase and surface conditions deteriorate, the bridge impact factors increase considerably. Such

behavior agrees with most previous researches regarding vehicle bridge interaction. The hypothetical straight bridge model cases show that the curvature also plays an important part in such dynamic interaction; curved models generally have a higher dynamic response than the straight versions [14]. A detail parametric study is required to understand how each factor contributes to the vehicle bridge interaction problem.

5. Parameter study

This parameter study focuses on following span variables in the vehicle bridge interaction system.

Three spans – 50m, 75m, 50m long.
Three spans – 35m, 50m, 35m long.
Three spans – 70m, 95m, 70m long.
Two spans – 95m each span.
Two spans – 75m each span.
Two spans – 50m each span.

Each of the above bridges was configured as curved bridges with radii of 50m, 75m, 100m, 150m, 190m, 250m, 300m, respectively, and one additional straight bridge case for comparison, resulting in 48 bridge configurations. Both concrete and steel curved bridges were studied in this research. But only the parametric study for steel bridges are demonstrated here. A set of steel box girders is design for the parameter study in order to represent the most widely used bridge type in the United States. These bridge cross sections need to be designed first according to the AASHTO LRFD code [18] and design standard using DESCUS-II@ [19] for box girder bridges.

Four sets of surface pavement conditions were integrated in the above bridge models, perfect, good, normal and bad conditions. The roughness ratio of these surface conditions are a=0, $0.24\times10^{-6}\leq a\leq1.0\times10^{-6}$, $1.0\times10^{-6}\leq a\leq4.0\times10^{-6}$ and $4.0\times10^{-6}\leq a\leq16.0\times10^{-6}$, respectively.

Three sets of lane configuration were integrated in the bridge models, vehicle travel in center lane e=0m, vehicle travel in inner lane e=-3.0m and vehicle travel in outer lane e=+3.0m. Each lane has a test vehicle travelling from 20m/s to 70m/s through the bridge. Combining the surface conditions and lane configurations, there are 576 model configurations in this study.

The results of the interaction analysis are evaluated by comparing the mid-span dynamic responses with the static responses. In the case of curvature radii study, it can be noticed how the dynamic interaction is influenced by the curvature. As the radius increases, both static and dynamic displacement responses are lowered, while the differences of dynamic and static responses also decline and start to stabilize after reaching R=150m. The difference (%) can be defined as [17]:

$$Difference = \frac{d_D - d_S}{d_S} \times 100\% \tag{10}$$

Where d_D is the maximum absolute displacement for center span mid-point under dynamic vehicle load, and d_S is the corresponding displacement under the same vehicle static load. Such

displacement difference percentage can be also considered as the dynamic amplified factor (impact factor) during vehicle bridge interaction. When radius is larger than 190m, the displacement impact factor stays around 7% to 9%. From curvature radii R=190m to R=50m, the maximum dynamic displacement response as well as the displacement dynamic impact factor increase rapidly. For the bridge configuration whose radius is 50m, the impact factor is 19.43%, 2.5 times of the impact factor (7.8%) from the original bridge configuration (Figure 7).

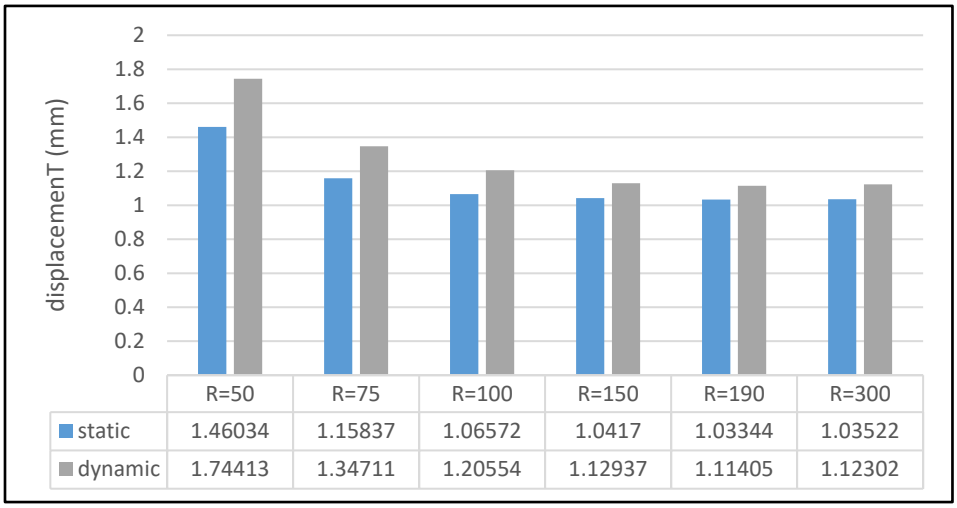

Fig. 7. Displacement response with different radii.

From Figures 8 to 9, the bridge moment response, like the displacement response, has a relatively less influence in cases where the curvature radii are higher. When the radii drop below R=150m, both the positive and negative moment responses start to react dramatically, especially when the radius reach R=50m.

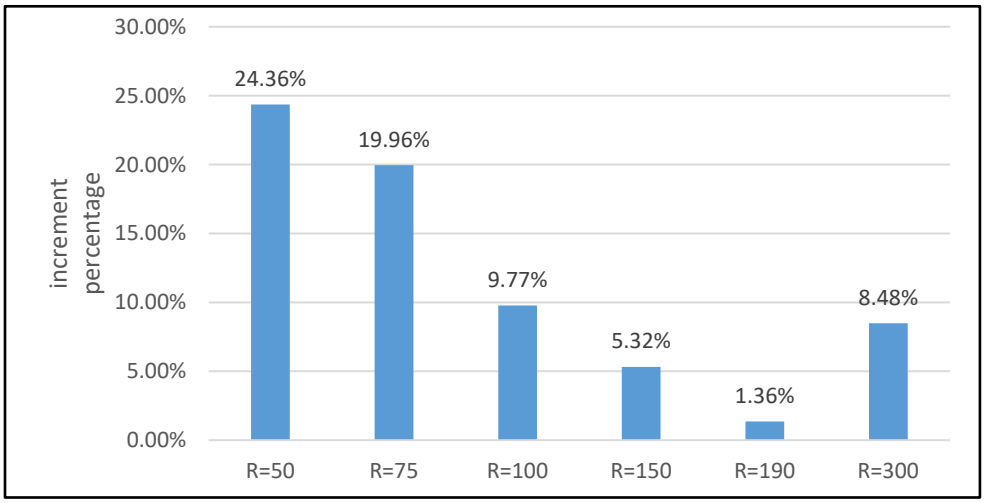

Fig. 8. Negative moment impact factors for different radii configurations.

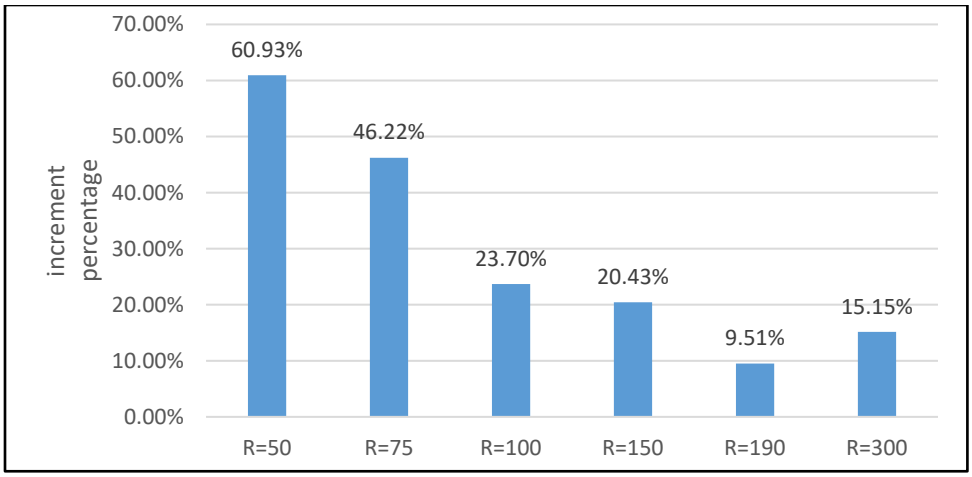

Fig. 9. Positive moment impact factors for different radii configurations.

Bridge responses from three different span lengths are gathered to study the influence of span length in vehicle bridge interaction. Figures 10 summarizes the maximum displacements and displacement impact factors of different configurations. Generally, with the increasing of span length, the bridge flexibility also increases. Bridge starts to increase the capability to absolve dynamic impact and reduce its effect on structure, thereafter, has lowered the impact factors. In these parametric study cases, it can be observed that, though the maximum static displacements increase with the span length, dynamic displacements do not have a higher increment rate, which leads to lower impact factor.

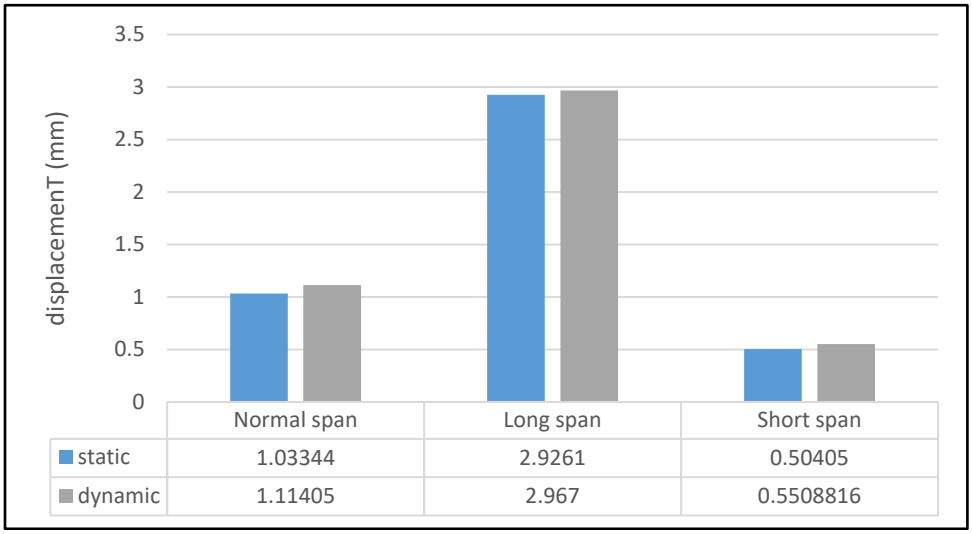

Fig. 10. Mid-span displacement comparison under different span length configurations.

Following Table 1 and Figure 11 summarize the influence of bridge surface condition to the vehicle bridge interaction analysis. It can be easily observed that with “Perfect” and “Good” surface conditions, the impact factors are below 10% and 20%, respectivily. With the deteriating of the bridge surface, the dynamic impact load increases dramatically. When the surface condition reaches “Bad”, the impact factor could be as high as 99%, even though the vehicle

traveling speed is still low. At such case, a near-resonance vibration is probably to happen which leads to a unusually high response.

Table 1
Impact factors (If) and Amplication factors (1+If) of different surfaces and span configurations.

table of impact factor	surface condition			
	Perfect	Good	Normal	Bad
Long span bridge	1.014 1.40%	1.066 6.61%	1.090 9.05%	1.200 19.98%
Normal span bridge	1.078 7.80%	1.108 10.78%	1.525 52.53%	1.994 99.37%
Short span bridge	1.093 9.29%	1.195 19.54%	1.534 53.40%	1.783 78.28%

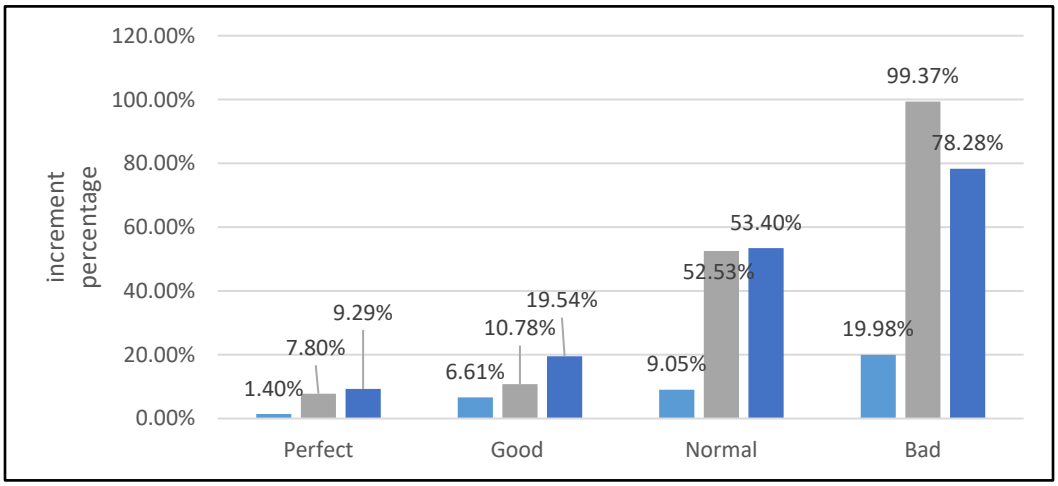

Fig. 11. Impact factor of different surfaces and span configurations.

A comparison is made in Figure 12 for eccentricity influence in vehicle bridge interaction. It can be observed that though generally the outer lane loading leads to higher impact factor, the difference in outer lane impact factor and inner lane impact factor is hardly noticeable compared to other factors such as speed and surface conditions.

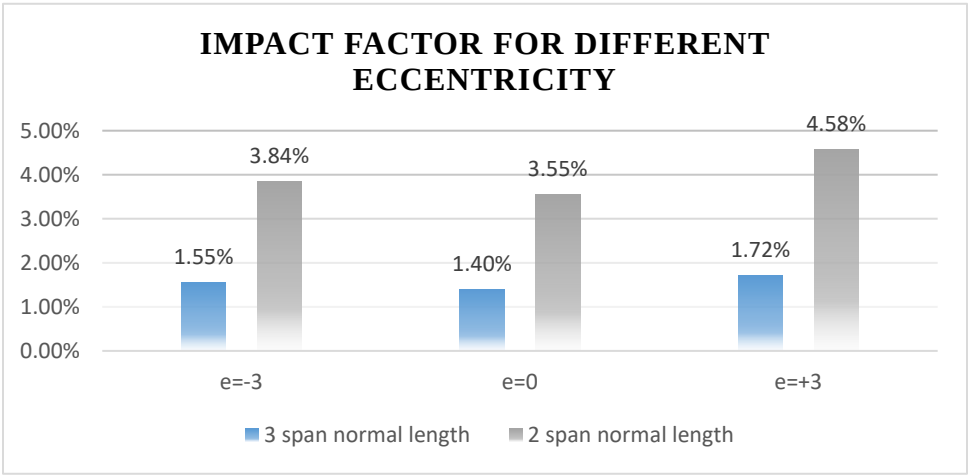

Fig. 12. Impact factor for different eccentricity.

6. Formulas of impact factor

From previous parametric study, the dynamic interaction usually leads to higher dynamic load than static loading. Factors such as the surface conditions can have a decisive and random influence on the dynamic interaction analysis. The location of maximum dynamic response can occur at various points and different static response locations. Therefore, in this study, the maximum displacement during the interaction period is selected for the impact factor calculation. The empirical formula for impact factor is categorized by the bridge surface conditions and bridge speed limits. The bridge material and geometric property can be simplified with the bridge fundamental flexural frequency in the empirical formula.

The displacement impact factor (I) can be expressed by the bridge frequency (ν) as follows:

a. For low speed limit bridge design

$$I = \begin{cases} 0.0067 + 0.087\nu \ \ (0.5 \le \nu \le 2) \\ 0.18 \ \ (2 \le \nu \le 4) \end{cases} \tag{11}$$

b. For high speed limit bridge design

$$I = \begin{cases} 0.09 + 0.07\nu \ \ (0.5 \le \nu \le 2) \\ 0.23 \ \ (2 \le \nu \le 4) \end{cases} \tag{12}$$

c. For low speed limit bridge service

$$I = \begin{cases} 0.027 + 0.097\nu \ \ (0.5 \le \nu \le 2) \\ 0.221 \ \ (2 \le \nu \le 4) \end{cases} \tag{13}$$

By comparing different impact factor equations, it can be observed that displacement impact factors trend to be the highest among these dynamic factors. A comparison of different determining methods of displacement impact factor is summarized in Figure 13. The AASHTO LRFD Bridge Design specifications 2017 considers most of the bridge components has a constant dynamic impact factor set of 0.33 and 0.15, regardless of bridge configurations [18]. While Canadian codes OHDBC 1982 and CHBDC 2000 both show similar impact factor developing trend as the current research, the impact factors increase as the bridge flexural frequency increases. All three impact factor determining methods have their fix maximum points for the impact factor. However, as this study shows, the impact factor is heavily influenced by the bridge surface condition. As the bridge deck starts wearing off during the service period, the impact factor will rise rapidly and most likely grow beyond the limits set by AASHTO and OHDBC codes.

There are multiple factors that affect the dynamic interaction in curved bridges. Another well accepted way to represent the curved bridge property is to introduce curvature central angle (ϕ=L/R) in the formula. Similar to previous formula, this empirical formula for impact factor is categorized by bridge surface conditions and bridge speed limits. The bridge material and geometric property can be simplified as the bridge central angle in the empirical formula.

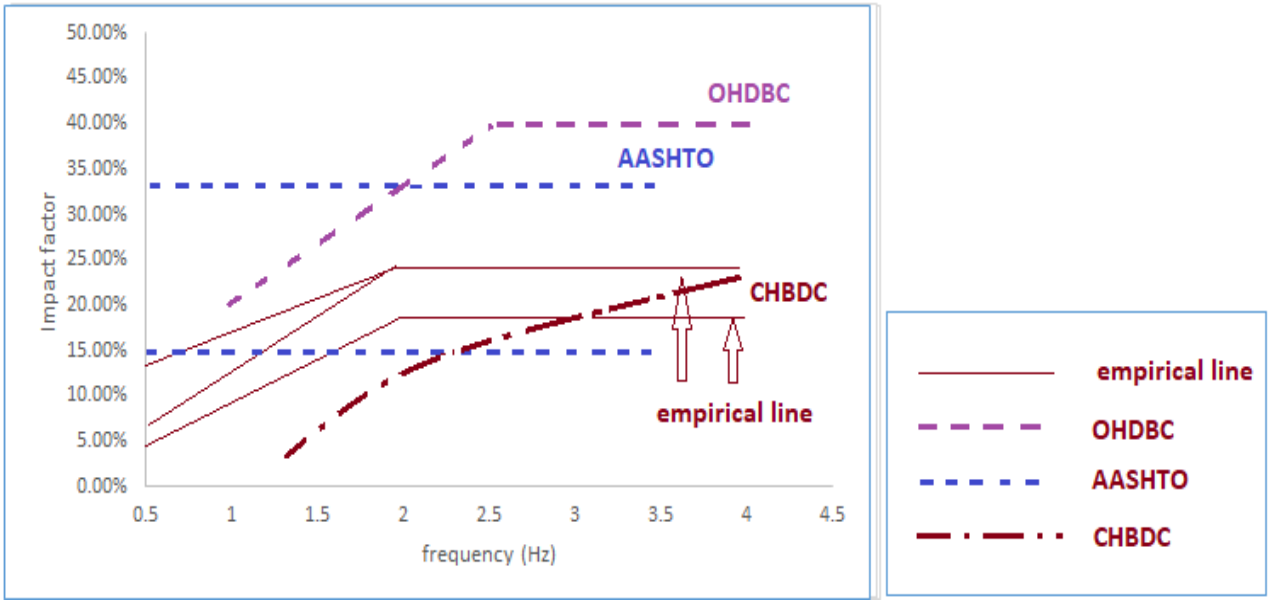

Fig. 13. Comparison of different methods of determining impact factor.

The displacement impact factor (I) can be expressed by the central angle (ϕ) in radian as follows:

a. For low speed limit bridge design

$$I = \begin{cases} 0.05 + 0.12\phi \ (0 \le \phi \le 1.25) \\ 0.20 \ (1.25 \le \phi \le 2.5) \\ 0.28625 - 0.0345\phi \ (2.5 \le \phi \le 4.0) \end{cases} \quad (14)$$

b. For high speed limit bridge design

$$I = \begin{cases} 0.10 + 0.0833\phi \ (0 \le \phi \le 1.5) \\ 0.225 \ (1.5 \le \phi \le 2.5) \\ 0.3 - 0.03\phi \ (2.5 \le \phi \le 4.0) \end{cases} \quad (15)$$

c. For low speed limit bridge service

$$I = \begin{cases} 0.15 + 0.10\phi \ (0 \le \phi \le 1.0) \\ 0.25 \ (1.0 \le \phi \le 2.5) \\ 0.367 - 0.0467\phi \ (2.5 \le \phi \le 4.0) \end{cases} \quad (16)$$

The empirical formulas generated above are a simplified supplementary method in addition to the previous frequency-depended method. In the cases of curved bridge problem, the central angle of the bridge can better account for the effect of bridge curvature property. From the parametric studies, it can be observed that when the bridge central angle sits around 1.0 to 2.5, the impact factor reaches its highest point. After ϕ=2.5, the impact factor steadily reduces. Combining the experience from parametric study, this indicates that when the ϕ is small, as the curvature radius decreases, the dynamic response increases dramatically, when the ϕ reaches beyond 2.5, as the span length increases, the dynamic interaction starts to gradually decline.

7. Conclusions

This paper develops an improved three-beam gird model based on shear-flexibility grillage analyzing method. Based on commercial software ANSYS Mechanical APDL command interface, the interaction system is modeled as a three-beam gird bridge model and a 24 degree-of-freedom 3-dimension truck model. These two subsystems are connected using simplified discrete iterative algorithm. The effects, such as bridge deck conditions and traffic speed, are introduced in the iterative algorithm and discussed extensively to study their influence in the vehicle-bridge interaction problem.

This paper proposed two empirical formulas for impact factor calculation based on the massive data from different bridge configurations and vehicle traveling patterns. By observing these, the upper bound envelop curve of impact factor is summarized. Based on such curve, a set of simple empirical equations is made for the calculation of curved bridge impact factor. By comparing to the current design specifications, the empirical equations show certain degree of agreement in the lower bridge flexural frequency range. However, none of the current codes sufficiently consider the extra dynamic load introduced by a dilapidated surface condition. During the parametric study, it can be frequently observed that the displacement impact factor climbs beyond the 0.75, which is the highest allowance provided in current design codes. Also, the highway speed limit is ignored in current codes, for the highway where speed limit is lower than 20m/s (45mph), the current codes will yield a much conservative result.

References

[1] Yang YB, Yau JD, Wu YS. Vehicle-Bridge Interaction Dynamics With Applications to High-Speed Railways. World Sci Publ Co 2004.

[2] Marcondes J, Burgess GJ, Harichandran R, Snyder MB. Spectral Analysis of Highway Pavement Roughness. J Transp Eng 1991;117:540–9. doi:10.1061/(ASCE)0733-947X(1991)117:5(540).

[3] Yang Y-B, Liao S-S, Lin B-H. Impact Formulas for Vehicles Moving over Simple and Continuous Beams. J Struct Eng 1995;121:1644–50. doi:10.1061/(ASCE)0733-9445(1995)121:11(1644).

[4] Zhou S, Song G, Wang R, Ren Z, Wen B. Nonlinear dynamic analysis for coupled vehicle-bridge vibration system on nonlinear foundation. Mech Syst Signal Process 2017;87:259–78. doi:10.1016/j.ymssp.2016.10.025.

[5] Huang D. Dynamic Analysis of Steel Curved Box Girder Bridges. J Bridg Eng 2001;6:506–13. doi:10.1061/(ASCE)1084-0702(2001)6:6(506).

[6] Hwang E, Nowak AS. Simulation of Dynamic Load for Bridges. J Struct Eng 1991;117:1413–34. doi:10.1061/(ASCE)0733-9445(1991)117:5(1413).

[7] YANG Y-B, WU C-M, YAU J-D. Dynamic response of a horizontally curved beam subjected to vertical and horizontal moving loads. J Sound Vib 2001;242:519–37. doi:10.1006/jsvi.2000.3355.

[8] Ding H, Shi K-L, Chen L-Q, Yang S-P. Dynamic response of an infinite Timoshenko beam on a nonlinear viscoelastic foundation to a moving load. Nonlinear Dyn 2013;73:285–98. doi:10.1007/s11071-013-0784-0.

[9] Cai C, He Q, Zhu S, Zhai W, Wang M. Dynamic interaction of suspension-type monorail vehicle

and bridge: Numerical simulation and experiment. Mech Syst Signal Process 2019;118:388–407. doi:10.1016/j.ymssp.2018.08.062.

[10] Mehmood A, Khan AA, Mehdi H. Vibration analysis of beam subjected to moving loads using finite element method. IOSR J Eng 2014;4:7–17.

[11] Zeng Q, Yang YB, Dimitrakopoulos EG. Dynamic response of high speed vehicles and sustaining curved bridges under conditions of resonance. Eng Struct 2016;114:61–74. doi:10.1016/j.engstruct.2016.02.006.

[12] Sennah KM, Zhang X, Kennedy JB. Impact Factors for Horizontally Curved Composite Box Girder Bridges. J Bridg Eng 2004;9:512–20. doi:10.1061/(ASCE)1084-0702(2004)9:6(512).

[13] Fafard M, Bennur M, Savard M. A general multi-axle vehicle model to study the bridge-vehicle interaction. Eng Comput 1997;14:491–508. doi:10.1108/02644409710170339.

[14] MARCHESIELLO S, FASANA A, GARIBALDI L, PIOMBO BAD. Dynamics of multi-span continuous straight bridges subject to multi-degrees of freedom moving vehicle excitation. J Sound Vib 1999;224:541–61. doi:10.1006/jsvi.1999.2197.

[15] Wang T, Huang D. Cable-Stayed Bridge Vibration due to Road Surface Roughness. J Struct Eng 1992;118:1354–74. doi:10.1061/(ASCE)0733-9445(1992)118:5(1354).

[16] Liu C, Huang D, Wang T-L. Analytical dynamic impact study based on correlated road roughness. Comput Struct 2002;80:1639–50. doi:10.1016/S0045-7949(02)00113-X.

[17] Chang D, Lee H. Impact Factors for Simple-Span Highway Girder Bridges. J Struct Eng 1994;120:704–15. doi:10.1061/(ASCE)0733-9445(1994)120:3(704).

[18] AASHTO, Load Resistance and Factor Design: Bridge Design Specifications, American Association of State Highway and Transportation Officials, 2017 Eighth Edition. n.d.

[19] C. C. Fu, DESCUS II. Win-DESCUS User’s manual for Design and Analysis of Curved BOX-Girder, 2009. n.d.